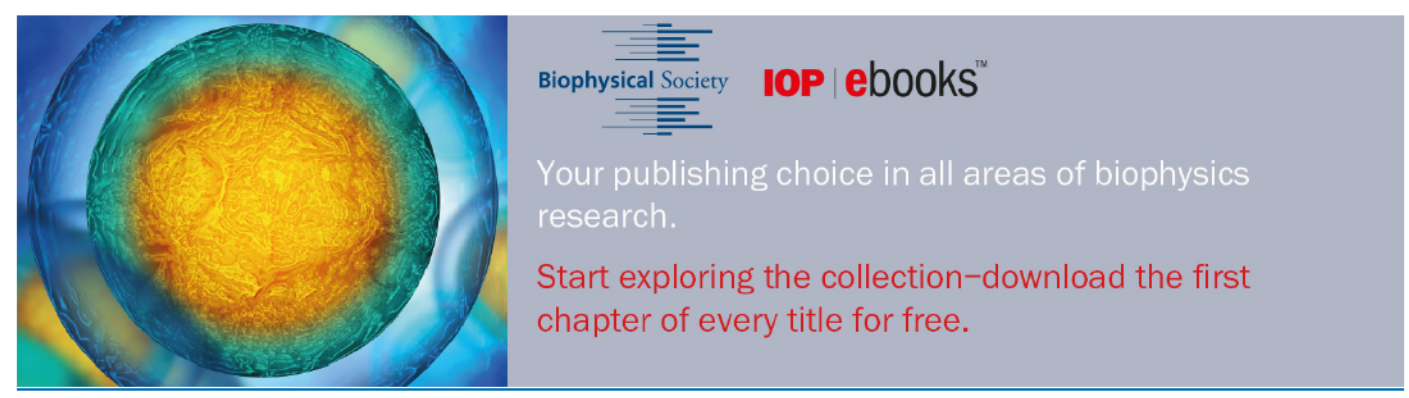
PAPER

Coulomb friction in twisting of biomimetic scale-covered substrate

To cite this article: Hossein Ebrahimi et al 2020 Bioinspir. Biomim. 15 056013

View the article online for updates and enhancements.



Bioinspiration & Biomimetics



RECEIVED 29 January 2020

REVISED 30 May 2020

ACCEPTED FOR PUBLICATION 23 June 2020

PUBLISHED 13 August 2020

PAPER

Coulomb friction in twisting of biomimetic scale-covered substrate

Hossein Ebrahimi[®], Hessein Ali[®] and Ranajay Ghosh[®]

Department of Mechanical and Aerospace Engineering, University of Central Florida, Orlando, FL 32816, United States of America

1 Author to whom any correspondence should be addressed.

E-mail: ranajay.ghosh@ucf.edu

Keywords: soft robotics, biomimetic, fish scale, interlocking, frictional dissipation

Abstract

Biomimetic scale-covered substrates provide geometric tailorability via scale orientation, spacing and also interfacial properties of contact in various deformation modes. No work has investigated the effect of friction in twisting deformation of biomimetic scale-covered beams. In this work, we investigate the frictional effects in the biomimetic scale-covered structure by developing an analytical model verified by finite element simulations. In this model, we consider dry (Coulomb) friction between rigid scales surfaces, and the substrate as the linear elastic rectangular beam. The obtained results show that the friction has a dual contribution on the system by advancing the locking mechanism due to change of mechanism from purely kinematic to interfacial behavior, and stiffening the twist response due to sharp increase in the engagement forces. We also discovered, by increasing the coefficient of friction potentially using engineering scale surfaces to a critical coefficient, the system could reach to instantaneous post-engagement locking. The developed model outlines analytical relationships between geometry, deformation, frictional force and strain energy, to design biomimetic scale-covered metamaterials for a wide range of applications.

1. Introduction

Many biological and biomimetic structures possess geometrically pronounced features. Such geometric features include for instance scales and intricate topological arrangement in their interior. This leads to nonlinear behavior such as nonlinear strain-stiffening in bending [1-5], nonlinear strain-stiffening in twisting [6], nonlinear stress-strain behavior in nature inspired cellular architecture [7-12], and nonlinear dispersion relationships in honeycomb structures leading to acoustic band gaps [13]. These structures include seashells, hierarchical honeycombs, snail spiral, seahorse tail, fish scales, lobster exoskeleton, crab exoskeleton, butterfly wings, armadillo exoskeleton, sponge skeleton, etc [10, 14-17]. Among these structures, dermal scales have garnered special attention recently due to complex mechanical behavior in bending and twisting [18-24]. Scales in nature are naturally multifunctional, lightweight [25-34], and protective of the underlying substrate, which has been an inspiration of armor designs [23, 24, 35, 36], where overlapping scales can resist penetration and provide additional stiffness [23, 24, 37, 38]. Fabrication

methods such as synthetic mesh sewing and stretchand-release have been recently developed to produce overlapping scale-covered structures in 2D and 1D configurations [39, 40]. These fabricated structures show almost ten times more puncture resistance than soft elastomers.

In addition to these localized loads, global deformation modes—such as bending and twisting—can be important for a host of applications that require structural modes of deformation, namely soft robotics, prosthetics, and morphing structures. In this context, characterizing bending and twisting plays an important role in ascertaining the benefits of these structures. Prior research has shown that bending and twisting of a scale-covered substrate show small-strain reversible nonlinear stiffening and locking behavior, due to the sliding kinematics of the scales embedded in the substrates [1-6, 41-45]. Such sliding interlocking structures possess certain unique characteristics, which give biological structures advantages without sophisticated parent materials. These include sharp and rapid increase in stiffness, leading to an almost rigid final shape (i.e. locking [2, 4-6]). This type of behavior is known to

assist the entire body of the fish as an external tendon [46, 47]. A good biological example here is the arapaima fish, which lives in the Amazon river, shown in figure 1(a). Their body's inner layer can twist and compress under stress, while their scales reorient themselves to help resist against external force and increase their strength [36, 48]. These dermal scales are also known to affect snake motion on surfaces [49–51]. Sliding behavior is also exploited in the tail of seahorses, which helps in its prehensile functionalities [52-54]. From an engineering perspective, such preferential locking behavior is critical for a range of applications. For example, in soft and collaborative robotics, a robotic appendage must balance flexibility and range of motion with stiffness to preserve an arm shape [55-57]. Thus, manipulating stiffening behavior is among the most important goals of such advanced applications.

Locked states guarantee the intermediate nonlinear behavior. Thus, the universality of such behaviors across deformation regimes needs to be ascertained. Several recent publications have probed this phenomena in depth for bending modes in both uniform [2] and non-uniform scales distributions [4, 5], and for both frictionless [2] and frictional cases [42]. However, the literature for the torsional deformation is somewhat less developed. Here, only the frictionless case has been probed into, which showed that locking is possible, but only for certain oblique angles of scales [6]. Therefore, the role of friction and its possible universal role has not been established in literature. In other words, questions remain about the parallels of properties modification brought about by friction in bending with twisting. For instance, Coulomb friction in bending regime advances the locking envelopes but at the same time, limits the range of operation [42]. In the dynamic regime, Coulomb friction can lead to damping behavior, which mimics viscous damping [44]. Clearly, friction between sliding scales can significantly alter the nature of nonlinearity. However, in spite of these studies, the role of friction in influencing the twisting behavior of a scale-covered structure has never been investigated before.

In this paper we investigate the role of friction in affecting the twisting behavior of biomimetic scale-covered systems under pure torsion for the first time. We establish an analytical model aided by finite element (FE) computational investigations. We assume rigid scales, linear elastic behavior of the substrate, and Coulomb model of friction between scales' surfaces. We compare our results with FE model to verify the proposed analytical model.

2. Materials and methods

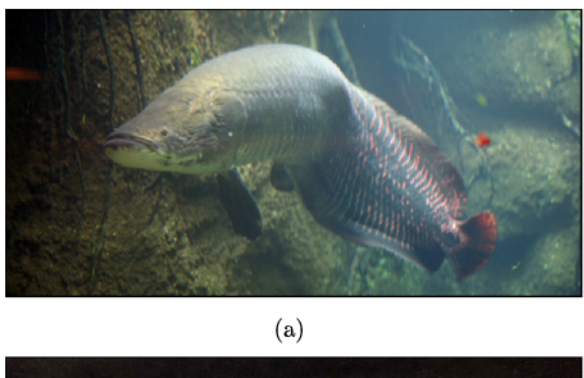
2.1. Materials and geometry

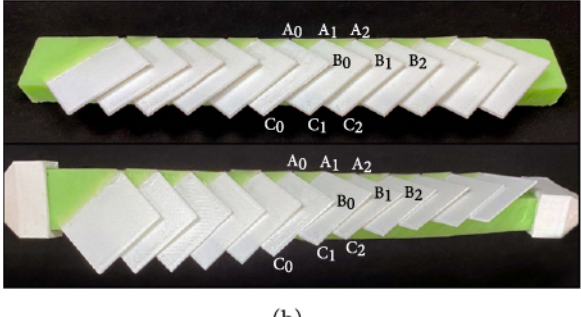
We consider a rectangular deformable prismatic bar with a row of rigid rectangular plates embedded on substrate's top surface. For the sake of illustration, we fabricate prototypes of 3D-printed scales made from the polymer Polylactic acid (PLA) ($E_{PLA} \sim 3$ GPa), partially embedded into the top surface of a silicone substrate and adhered with silicone glue (Permatex Corporate) to prefabricated grooves on the molded slender vinylpolysiloxane (VPS) (Zhermack SpA) substrate ($E_{VPS} \sim 1.5 MPa$), as shown in figure 1(b). The Young's modulus of these materials were obtained by tensile tests and the substrate's material was found to behave linearly for moderate torsional deformation [6]. In our lab scale testing, the silicone based polymeric substrate material did not exhibit appreciable anisotropy. This is consistent with previous reports in literature [58, 59]. However, for the biomimetic scale-covered substrate, anisotropy between directions of twisting (engaged vs non-engaged) would obviously arise. This is an example of emergent behavior, which is typical in many topologically and geometrically complex structures including the current system [11, 12]. The prototype is illustrated under twisted configuration in figure 1(b). The rigidity assumption for the scales is valid in the limit of much higher stiffness of the scales, away from the locking state [24, 46]. Note that we did not perform physical torsion experiments in this paper, but used real prototypes only for aiding visualization.

The pure twisting behavior allows us to assume periodicity, letting us isolate a fundamental representative volume element (RVE) for modeling the system, figure 2(a). The scales are considered to be rectangular rigid plates with thickness t_s , width 2b, and length l_s , and oriented at angles θ and α as shown in figure 2(b) with respect to the rectangular prismatic substrate. θ is the scale inclination angle defined as the dihedral angle between the substrate's top surface and the scale's bottom surface, and α is the angle between the substrate's cross section and the scale's width. The length of exposed section of scales is denoted as l, and the length of embedded section of the scales is L. Therefore, the total length of the scale is $l_s = L + l$. The spacing between the scales is constant and denoted by d, which is a geometrical parameter reciprocal to the density of scales. We assume that the scale's thickness t_s is negligible with respect to the length of the scales, $l_{\rm s}$ ($t_{\rm s} \ll l_{\rm s}$), and the scale's embedded length is also negligible with respect to the substrate's thickness $(0 \ll L \ll 2t)$. This thin-plate idealization for the biomimetic scales is appropriate for this case and typically used in literature for analogous systems [2, 4-6, 42-44].

2.2. Kinematics

For global deformation modes such as pure bending and twisting, the scale periodicity is a good approximation [2, 6]. Periodicity assumption allows us to consider just three consecutive scales configuration at the RVE level, we call these scales as 'zeroth scale',





(b)

Figure 1. (a) Arapaima fish which can twist their body's inner layer and their scales reorient themselves to help resisting against external force and increase their strength. The image has been adapted under CC BY 2.0 license [60]. (b) The fabricated prototype were made from 3D-printed polylactic acid scales and molded slender VPS substrate in initial and twisted configuration.

'1st scale', and '2nd scale', respectively, from left to right. The corners of these scales are marked likewise in figures 1(b) and 2. Without loss of generality, we consider 1st scale is fixed locally with respect to other scales. A twisting deformation with twist rate Φ , is applied to the rectangular prismatic substrate about torsion axis, which passes through the beam cross section center. Due to this underlying deformation, the 2nd scale rotates by the local twist angle of $\varphi = \Phi d$, and the zeroth scale rotates in reverse direction about the torsion axis with $-\varphi = -\Phi d$, because 1st scale assumed locally fixed. The continual twisting of the substrate progresses the contact between each two consecutive scales simultaneously due to periodicity, by coincidence between lines C_1B_1 and D_2C_2 , as well as lines D_1C_1 and C_0B_0 .

To find a contact criterion between 1st scale and 2nd scale, the 3D-equations of lines C_1B_1 and D_2C_2 would be established. We place the coordinates XYZ on the midpoint of 1st scale's width as shown in figure 2. Then we place coordinates xyz on the torsion axis at point O = (0, -t, 0) measured from the coordinates XYZ. Hereafter, coordinates xyz is our reference frame. Note that, we do not show coordinates xyz and scale's thickness t_s in figure 2(b) to avoid visual complexity. We establish local coordinates on each scale, denoted as 'local coordinates of ith scale', and coordinates origin is located on the corner of the scale at point D_i . In these local coordinates, the unit vector of x-axis (n_{Xi}) is on the edge D_iC_i , the unit vector of y-axis (n_{Yi}) is on the edge D_iA_i , and the unit vector of z-axis (n_{Zi}) is out of plane and perpendicular to n_{Xi} and n_{Yi} , figure 2(b). On each scale, edges D_iC_i

and A_iB_i are parallel and in direction of n_{Xi} , and edges C_iB_i and D_iA_i are parallel and in direction of n_{Yi} . Point M_i is located in the middle of edge C_iB_i . Using these established coordinates, equations of line C_1B_1 of 1st scale can be obtained on the base of the unit vector n_{Y1} and the location of point M_1 , which is located in the middle of the edge C_1B_1 . Line D_2C_2 is located on the 2nd scale, which is rotating with angle φ about torsion axis. To find the equation of this line, first we locate the corners of 2nd scale as shown in figure 2(a), before and after rotation using rotation matrix. Thus, we find the location of point D_2 and C_2 after rotation, which are located at ends of the line D_2C_2 . Then, the rotating local coordinates on this scale and the unit vector in direction D_2C_2 (n_{X2}) can be established. Finally, the equations of line D_2C_2 is delivered by using the unit vector n_{X2} and point D_2 .

To find the contact point of these two lines, we solve their equations together as a system of equations, which yields a nonlinear relationship between φ and θ . To represent a general form for this relationship, we define dimensionless geometric parameters $\eta = l/d$, $\beta = b/d$, and $\lambda = t/d$ as the overlap ratio, dimensionless scale width, and dimensionless substrate thickness, respectively. The governing relationship between the substrate local twist angle φ and the scale inclination angle θ can be written as:

$$(\cos \varphi - 1) \left(\beta \sin 2\alpha \sin \theta + \eta \cos^2 \alpha \sin 2\theta \right)$$

$$+ 2\lambda \cos 2\alpha \cos \theta - 2 \cos \alpha \cos \varphi \sin \theta$$

$$+ 2 \sin \alpha \sin \varphi (\eta + \lambda \sin \theta)$$

$$+ 2 \cos \alpha \sin \varphi \cos \theta (\beta - \sin \alpha) = 0.$$
 (1)

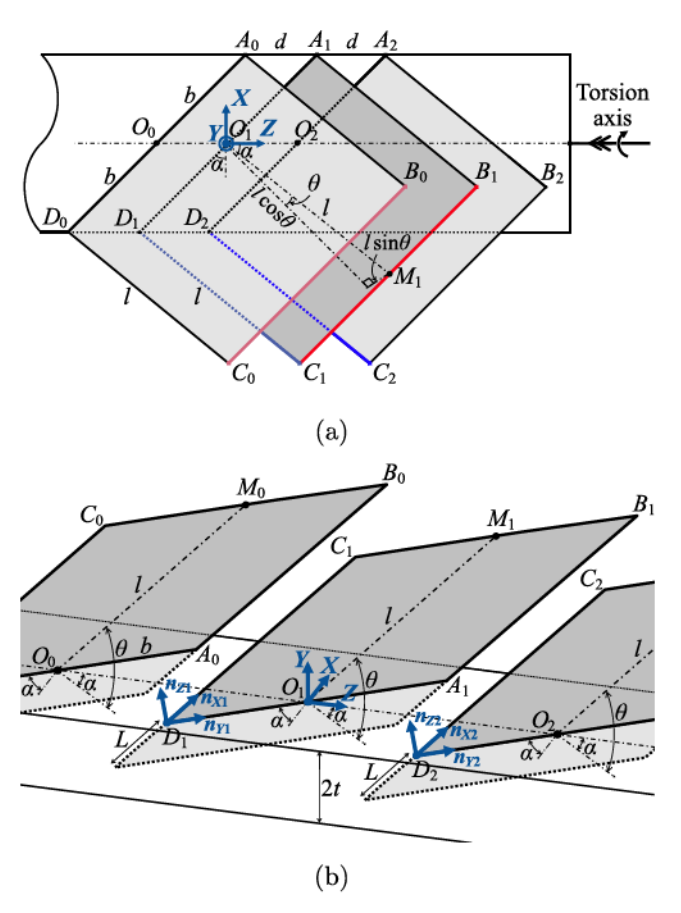


Figure 2. The schematic of three consecutive scales geometrical configuration: (a) top view of scales configuration. (b) Dimetric view showing scales orientational angles of θ and α , and the embedded part of the each scale. Note that angle θ is exaggerated and the scale's thickness t_s is not illustrated in this figure.

The details of derivation of this relationship can be found in appendix A. We can use the same procedure to establish the locations of zeroth scale's corners and its local coordinates after rotating with angle $-\varphi$ about torsion axis. We find the same nonlinear relationship between φ and θ as shown in equation (1) due to the periodicity of the system. Also, the location of point P_{12} as the intersection between lines D_2C_2 and C_1B_1 , and the location of point P_{10} as the intersection between lines D_1C_1 and C_0B_0 , can be calculated as described in appendix A. These points are illustrated in figure 3, which shows the twisted state of the RVE.

To express the dimensionless geometric parameters qualitatively in a biological scale-covered system, it can be mentioned that the overlap ratio $\eta = l/d$ determines how much fish scales are long, and $\beta = b/d$ is representing fish scales width. Also, $\lambda = t/d$ determines the thickness of the effective fish skin layer.

From the beginning of contact between the scales (scales engagement), the relationship (1) is established between the substrate local twist angle φ and the scales inclination angle θ . After starting the scales engagement, scales slide over each other and θ starts to increase from its initial value θ_0 according to the nonlinear relationship (1). Note that scales engagement starts at a point with relatively small local twist angle

which we call it engagement point (E_p) . Therefore, to find an explicit relationship for the local twist angle φ at this point known as the engagement twist angle φ_e , we linearize (1) by considering small twist regime $(\varphi \ll 1, \ \theta \ll 1)$ which leads to $\varphi_e = \theta_0/(\eta \tan \alpha + \beta - \sin \alpha)$.

Using the kinematic relationship (1), we probe the existence of a singular point where locking can take place. This would be the envelope defined by $\partial \varphi / \partial \theta = 0$, and beyond which no more sliding is possible without significant deformation of the scales. This point is called the 'kinematic locking' of the system [6]. The locking point (L_p) happens when the scale-covered structure, even though it has a deformable substrate, can not be twisted anymore due to the kinematic contact between relative-rigid scales (scales engagement) and the established geometrical arrangement (singular point). Note that the kinematic locking state can occur even without friction since it is a result of singularity in the governing kinematic relationship of the system. Beyond this point, stiffness increases sharply as it is determined by the stiffness of the scales.

2.3. Mechanics

To investigate the role of friction in twisting behavior of biomimetic scale-covered substrate, we investigate the free body diagram of the RVE (here 1st scale)

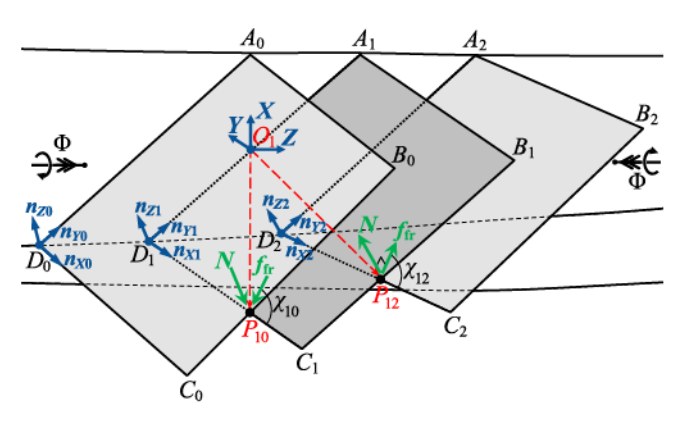


Figure 3. Twisted state of the RVE and free body diagram of each pair of scales representing their contact points P_{10} and P_{12} , normal force N, and friction force f_{fr} at the contact points.

during engagement as shown in figure 3. The forces on the 1st scale are as follows. At contact point between zeroth scale and 1st scale P_{10} , there are two reaction forces including friction force f_{10} acting in the plane of 1st scale by angle χ_{10} with respect to the unit vector n_{X1} , and normal force N_{10} acting perpendicular to this plane in direction $-n_{Z1}$ as shown in figure 3. Also, at contact point between 1st scale and 2nd scale P_{12} , two reaction forces are acting including friction force f_{12} in the plane of 2nd scale by angle χ_{12} with respect to the unit vector n_{X2} , and normal force N_{12} perpendicular to the plane of 2nd scale in direction n_{Z2} as shown in figure 3.

Note that the direction of friction forces are dependent on the direction of relative motion between each scale pairs. Due to the periodicity, the value of friction forces are equal $f_{\rm fr} = f_{10} = f_{12}$, and also the value of normal forces are equal $N = N_{10} = N_{12}$. According to the described free body diagram, the balance of moments at the base of 1st scale can be described in the vectorial format as follows:

$$K_{\theta}(\theta - \theta_{0}) = \left(O_{1}P_{10} \times \left(-(f_{\text{fr}}\cos\chi_{10})n_{X1}\right) - (f_{\text{fr}}\sin\chi_{10})n_{Y1} - (N)n_{Z1}\right) + O_{1}P_{12} \times \left((f_{\text{fr}}\cos\chi_{12})n_{X2} + (f_{\text{fr}}\sin\chi_{12})n_{Y2} + (N)n_{Z2}\right)\right).n_{Y1},$$
(2)

where O_1P_{10} and O_1P_{12} are the position vector of contact points P_{10} and P_{12} with respect to the base of

the 1st scale, respectively, as shown in figure 3. K_{θ} is the 'rotational spring constant' or the 'rigid scale-elastic substrate joint stiffness'. As the scales engage, they tend to push each other and increase their inclination angle θ , but the elastic substrate resists against scales rotation. This resistance is modeled as linear torsional spring [1, 2, 6], and the absorbed energy due to the rotation of each scale is $U_{\text{scale}} = \frac{1}{2} K_{\theta} (\theta - \theta_0)^2$, thus the local reaction moment would be $M_{\text{scale}} = K_{\theta}(\theta - \theta_0)$. According to developed scaling expression in [6], K_{θ} = $3.62E_{\rm B}t_{\rm s}^{\ 2}\ b(L/t_{\rm s})^{1.55}$, where $E_{\rm B}$ is the elastic modulus of substrate. According to the Coulomb's law of friction, scales do not slide while $f_{\rm fr} \leq \mu N$, where μ and N are coefficient of friction and normal force, respectively, while sliding regime is marked by the equality. Note that we use the same value for static coefficient of friction as well as the kinetic coefficient of friction in this study, although typically static coefficient of friction is slightly higher [61, 62]. On the basis of scales relative motion expressed in appendix B, the angle between the friction force $f_{\rm fr}$ in the 1st scale plane and the unit vector n_{X1} is equal to the angle between friction force $f_{\rm fr}$ in the 2nd scale plane and the unit vector n_{X2} . This means $\chi_{10} = \chi_{12}$, and can be shown as χ . This finding also conforms the periodicity in the system. Using these considerations, we can derive the following expression as the non-dimensionalized friction force \overline{f}_0 , with respect to the free body diagram shown in figure 3:

$$\overline{f}_0 = \frac{f_{\text{fr}}l}{K_{\theta}} \leq \frac{(\theta - \theta_0)l}{\left(O_1 P_{12} \times \left(\cos\chi n_{X2} + \sin\chi n_{Y2} + \frac{1}{\mu}n_{Z2}\right) - O_1 P_{10} \times \left(\cos\chi n_{X1} + \sin\chi n_{Y1} + \frac{1}{\mu}n_{Z1}\right)\right).n_{Y1}}.$$
(3)

Due to the nature and the geometrical configuration of the system, the magnitude of the friction

force derived in (3), may exhibit singularity at a certain twist rate. This rise in friction force may lead to a

'frictional locking' mechanism, observed in the bending case too [42]. If predicted, the frictional locking should happen at the lower twist rate compared to kinematic locking, because of the limiting nature of friction force. We call the twist rate in which locking happens as $\Phi_{\rm lock}$, and the local twist angle and the scale inclination angle would be as $\varphi_{\rm lock} = \Phi_{\rm lock} d$ and $\theta_{\rm lock}$, respectively.

The friction force computed above will lead to dissipative work in the system during sliding. The nondissipative component of the deformation is absorbed as the elastic energy of the biomimetic beam. This elastic energy is composed of elastic energy of the beam and the scales rotation. To calculate this elastic energy of the beam, we consider a linear elastic behavior for the beam with a warping coefficient C_w for a non-circular beam [6, 63]. Furthermore, due to the finite embedding of the scales, there will be an intrinsic stiffening of the structure even before scales engagement. This stiffening can be accurately captured by using an inclusion correction factor C_f [6]. C_f is a function of the volume fraction of the rigid inclusion into the elastic substrate, and postulated as $C_f = 1 + 1.33(\zeta \beta/\lambda)$, where $\zeta = L/d$ for an analogous system [6]. With these considerations, modified torque-twist relationship of the beam is $T = C_f C_w G_B I \Phi$, and the elastic energy of the beam can be considered as $U_{\rm B} = \frac{1}{2} C_{\rm f} C_{\rm w} G_{\rm B} I \Phi^2$. As mentioned earlier, the energy absorbed by the scales can be obtained by assuming the scale's resistance as linear torsional spring and the absorbed energy due to the rotation of each scale will be $U_{\text{scale}} = \frac{1}{2} K_{\theta} (\theta - \theta_0)^2$. Similarly the dissipation can be given as the product of the sliding friction and distance traveled by the point of application per scale. Then we use the work-energy balance to

$$\int_0^{\Phi} T(\Phi') d\Phi' = \frac{1}{2} C_f C_w G_B I \Phi^2 + \left(\frac{1}{2} \frac{1}{d} K_{\theta} (\theta - \theta_0)^2 + \frac{1}{d} \int_{\Phi_e}^{\Phi} f_{fr} dr \right) H(\Phi - \Phi_e), \tag{4}$$

where Φ , $\Phi_{\rm e}=\varphi_{\rm e}/d$, $G_{\rm B}$, and I are the current twist rate, the engagement twist rate, the shear modulus of elasticity, and the beam cross section's moment of inertia. $H(\Phi-\Phi_{\rm e})$ is the Heaviside step function to track scales engagement. Also, $C_{\rm f}$, $C_{\rm w}$, and K_{θ} are inclusion correction factor, warping coefficient, and rotational spring constant of scale—substrate joint stiffness, respectively. In (4), $f_{\rm fr}$ represents the friction force between scales, and dr is the relative differential displacement traveled by the point of friction application. Derivation of dr has been described in appendix B.

The torque–twist rate relationship per substrate's unit length could be obtained by taking the derivative of (4) with respect to the twist rate Φ , while considering $\varphi = \Phi d$, as follows:

$$T(\Phi) = C_{\rm f} C_{\rm w} G_{\rm B} I \Phi + \left(K_{\theta} (\theta - \theta_0) \frac{\partial \theta}{\partial \varphi} + f_{\rm fr} \frac{\mathrm{d}r}{\mathrm{d}\varphi} \right)$$
$$\times H(\Phi - \Phi_{\rm e}). \tag{5}$$

We also compute the maximum possible dissipation of the system by computing the frictional work done till locking ($W_{\rm fr}$) and compare it with the total work done ($W_{\rm sys}=U_{\rm el}+W_{\rm fr}$, where $U_{\rm el}$ is the elastic energy of the system). These energies can be computed per substrate's unit length as:

$$U_{\rm el} = \frac{1}{2} \left(C_{\rm f} C_{\rm w} G_{\rm B} I(\Phi_{\rm lock})^2 + \frac{1}{d} K_{\theta} (\theta_{\rm lock} - \theta_0)^2 \right), \tag{6a}$$

$$W_{\rm fr} = \frac{1}{d} \int_{\Phi_e}^{\Phi_{\rm lock}} f_{\rm fr} \mathrm{d}r. \tag{6b}$$

We define the relative energy dissipation (RED) factor as the ratio of the frictional work per unit length $W_{\rm fr}$, to the total work done on the system per unit length $W_{\rm sys}$:

$$RED = \frac{W_{fr}}{W_{sys}}. (7)$$

Generally, RED is dependant on the coefficient of friction μ , dimensionless geometric parameters of the system η , β , and λ , scale spacing d, scales initial orientation angles α and θ_0 , substrate elastic properties $G_{\rm B}$, I, and $C_{\rm w}$, and scale—substrate joint parameters K_{θ} and $C_{\rm f}$, but the most important parameters are μ , η , and α .

3. Finite element simulations

We have developed an FE model for verification of the developed analytical model for the biomimetic scalecovered system under twisting deformation. The FE simulations are carried out using commercially available software ABAQUS/CAE 2017 (Dassault Systèmes). We considered 3D deformable solids for scale and substrate. However, for the scales, rigid body constraint was imposed. A sufficient substrate length is considered for rectangular prismatic substrate to satisfy the periodicity. Then an assembly of substrate with a row of 25 scales embedded on its top surface is created. The scales are oriented at angles of θ_0 and α as defined in the analytical model. Linear elastic material properties including $E_{\rm B}$ and ν are applied to the substrate part which leads to the shear modulus of $G_{\rm B}=\frac{E_{\rm B}}{2(1+\nu)}$.

The simulation was considered as a static step with nonlinear geometry option. The left side of the beam is fixed and the twisting load was applied on the other side of the beam. A frictional contact criteria is applied to the scales surfaces with coefficient of friction μ for a twisting simulation. The top layer of substrate is meshed with tetrahedral quadratic elements C3D10 due to the geometrical complexity

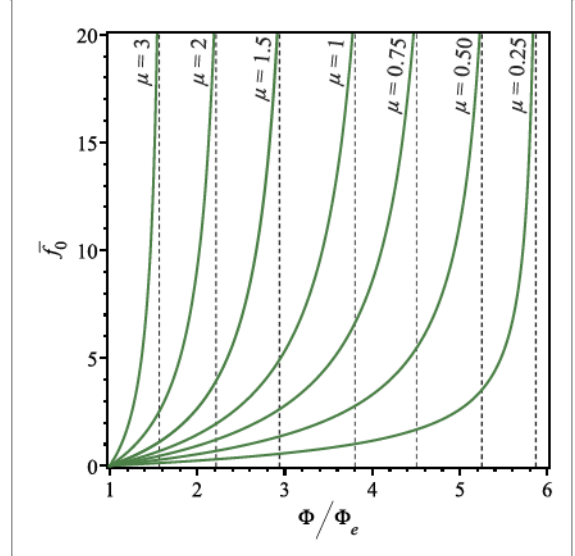


Figure 4. Non-dimensionalized friction force vs non-dimensionalized twist rate ($\Phi_{\rm e}$ is the engagement twist rate) for various coefficients of friction with the given values of $\eta=3,\,\theta_0=10^\circ,\,\alpha=45^\circ,\,\beta=1.25,$ and $\lambda=0.45.$ This figure shows that the friction forces approach singularity near a certain twist rate as the frictional locking configuration for each μ .

around scales inclusion. Quadratic hexahedral elements C3D20 are used for other regions of the model. A mesh convergence study is carried out to find sufficient mesh density for different regions of the model. A total of almost 70 000 elements are employed in the FE model.

4. Results and discussion

To study the frictional force behavior in this system, we use (3) to plot non-dimensionalized friction force \overline{f}_0 for different μ values at various non-dimensionalized twist rate Φ/Φ_e . In a real biological scale-covered system like fish scales, the geometry of fish scales, scales' surface roughness, and the epidermal mucus, which typically covers the fish scales, significantly affect the values of coefficient of friction μ [64]. The non-dimensionalized friction force is shown in figure 4 for scale-covered system with $\eta = 3$, $\theta_0 = 10^\circ$, $\alpha = 45^\circ$, $\beta = 1.25$, and $\lambda =$ 0.45. From this figure, it is clear that increasing twist rate leads to a rapid increase in the friction force for any coefficient of friction. There is a singular characteristic for this load as shown with dashed lines for each μ in figure 4, which indicates a friction-based locking mechanism. This is in addition to the purely kinematic locking mechanism reported earlier in literature for frictionless counterparts [6]. We call the twist rate at the locking point (L_p) , as the locking twist rate Φ_{lock} .

Next, we investigate the scale rotation in response to applied twist. This is achieved by plotting the scale inclination angle θ versus substrate local twist angle φ . Using the nonlinear relationship (1), two plots are

established spanned by $(\theta-\theta_0)/\pi$ and φ/π as shown in figure 5 for different η and α , respectively. Note that in a biological fish scales system, η roughly translates to the extent of scales overlap. Whereas, α describes the angle between the direction of scales arrangement and the twist axis.

In figure 5(a), the given geometrical parameters are as follows $\theta_0 = 10^{\circ}$, $\alpha = 45^{\circ}$, $\beta = 1.25$, and $\lambda = 0.45$. For $\mu = 0$, which indicates frictionless case, we obtain purely kinematic locking points for each η by using $\partial \varphi / \partial \theta = 0$ to obtain rigidity envelope [6]. We juxtapose this with plots of the rough interfaces $(\mu > 0)$, where the locking limits are found via the singularity point of friction force described in (3). Clearly, friction advances the locking configuration. However, the locking line does not merely translate downwards as observed in the bending case [42]. This is an important distinction from the pure bending of rough biomimetic scale-covered beams reported earlier [42]. As coefficient of friction increases, the frictional locking envelope can intersect the horizontal axis. This is the instantaneous locking or the 'static friction locking' case. Interestingly, this is a geometrically-dictated static friction locking in contrast to the actual static friction coefficient mediated locking. This once again highlights the contrast and interplay of material and geometry in this class of structures.

In figure 5(b), the effect of scales orientation with angle α is investigated. This angle serves as an important geometric tailorability parameter of the system [6]. In this plot, $\eta = 3$, $\theta_0 = 10^\circ$, $\beta = 1.25$, and $\lambda = 0.45$. For higher angles α , a quicker engagement occurs with steeper nonlinear gains and earlier locking. As shown in figure 5(b), the curves for lower α ($\alpha = 15^{\circ}$ and $\alpha = 0^{\circ}$) fail to reach the rigidity envelope for $\mu = 0$, because mathematically there is no singularity point for equation (1) for these cases. This means, by decreasing α sufficiently, the system would not reach to the kinematic locking. However, frictional locking is universal and will determine the locking behavior. In this aspect, this system again differs from bending case, since in twisting, friction can cause locking even when kinematic locking is not possible. This figure also shows the possibility of static friction locking by increasing μ . However, note that as α increases, such static friction locking becomes more difficult to achieve, because it requires much higher frictional coefficients. Overall, the frictional locking envelope is a highly nonlinear function admitting no closed form solution unlike the pure bending case [42].

In order to understand the effect of friction force on the mechanics of the system, we use (5) to plot the non-dimensionalized post-engagement torque—twist rate plot for various coefficients of friction, figure 6(a). Dimensionless geometrical parameters for this case are $\eta = 3$, $\theta_0 = 10^\circ$, $\alpha = 45^\circ$, $\beta = 1.25$, $\lambda = 0.45$, $\zeta = 0.35$, and $L/t_s = 35$. As

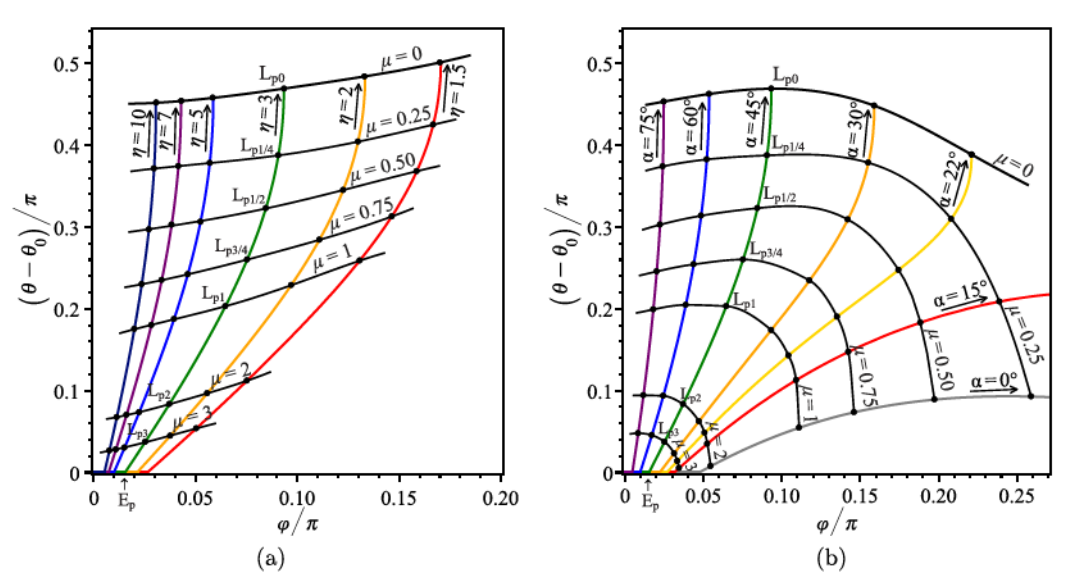


Figure 5. The plot representation of the biomimetic scale-covered beam under twisting differentiated to three distinct regimes of performance including: linear region (before scales engagement) which is from 0 to engagement point (E_p) shown on e.g. curves $\eta=3$ and $\alpha=45^\circ$; nonlinear region (during scales engagement) which is from engagement point (E_p) to locking point for $\mu=k$ (E_p) shown on e.g. curves $\eta=3$ and $\alpha=45^\circ$; and rigid region which is after locking point for $\mu=k$ (E_p) shown on e.g. curves $\eta=3$ and $\alpha=45^\circ$. (a) Plot of the system for different η with the given values of $\theta_0=10^\circ$, $\alpha=45^\circ$, $\beta=1.25$, and $\lambda=0.45$; and (b) plot of the system for different α with the given values of $\eta=3$, $\theta_0=10^\circ$, $\beta=1.25$, and $\lambda=0.45$.

shown in figure 6(a), higher coefficient of friction significantly increases the torsional stiffness of the structure. Therefore, the friction force has a dual contribution to the mechanical response of the biomimetic scale-covered system—while advancing locking state, thereby limiting range of motion, but also increasing the torsional stiffness of the system.

To verify the analytical model, we have developed an FE model as described in section 3. Then we have performed FE simulations for different η and μ values and extracted torsional response of the structure $T(\Phi)/G_BI$, versus twist rate from the beginning of the simulation as shown in figure 6(b). The following dimensionless parameters are used for this model: $\theta_0 = 10^{\circ}$, $\alpha = 45^{\circ}$, $\beta = 0.6$, $\lambda = 0.32$, $\zeta = 0.18$, and $L/t_s = 45$. Also the following elastic properties are considered for substrate: $E_B = 25$ GPa, $\nu = 0.25$, with a cross section dimension of 32 × 16 mm. In this figure, the dotted lines represent FE results. The plot highlights remarkable agreement between analytical and FE results for two different overlap ratios along with different coefficients of friction. The small deviation between results could be caused by edge effects and numerical issues. As it is shown in figure 6(b), we have performed multiple FE simulations for different cases. We have presented a contour plot of von Mises stress with real-scale deformation for one of these cases in appendix C to give a better perspective about the FE investigations which have been performed in this work.

Note that there are differences in visual appearance between these two torque-twist curves (figures 6(a) and (b)). This is not mutually contradictory. The figure 6(a) captures the twisting

response only after the scale engagement, which visually amplifies the nonlinearity, whereas figure 6(b) plots from the reference configuration. Since figure 6(b) captures only a small portion of the nonlinearity, it appears visually linear after engagement. Due to extreme convergence issue with FE software used for model verification, we are limited to relatively small twisting angles. The excellent match between FE and model is due in part to model accuracy, and also the relatively small geometric nonlinearity affecting the FE simulations. We expect significantly more deviations from the theory if the twisting were to proceed to relatively large values or near locking where scale deformations would be significant.

As we have mentioned earlier in section 2.3, we have considered the same value for static and kinetic coefficient of friction in this study, but in general the coefficients of static friction μ_s and kinetic friction μ_k are always slightly different, with $\mu_s > \mu_k$ [61, 62]. From the mechanics point of view, vastly different coefficients of friction can lead to jumps in torque-twist behavior after initial contact is made. Thus, the twisting motion will momentarily stop till the applied torque leads the internal forces to a sufficient value to overcome static friction. At this point, the motion will start again and resume on the path calculated from kinetic friction assumption. This can lead to a momentary stick-slip motion. Once sliding begins again, the rest of the plot would be similar.

Only a fraction of applied work goes into elastic storage, whereas the rest is dissipated or lost.

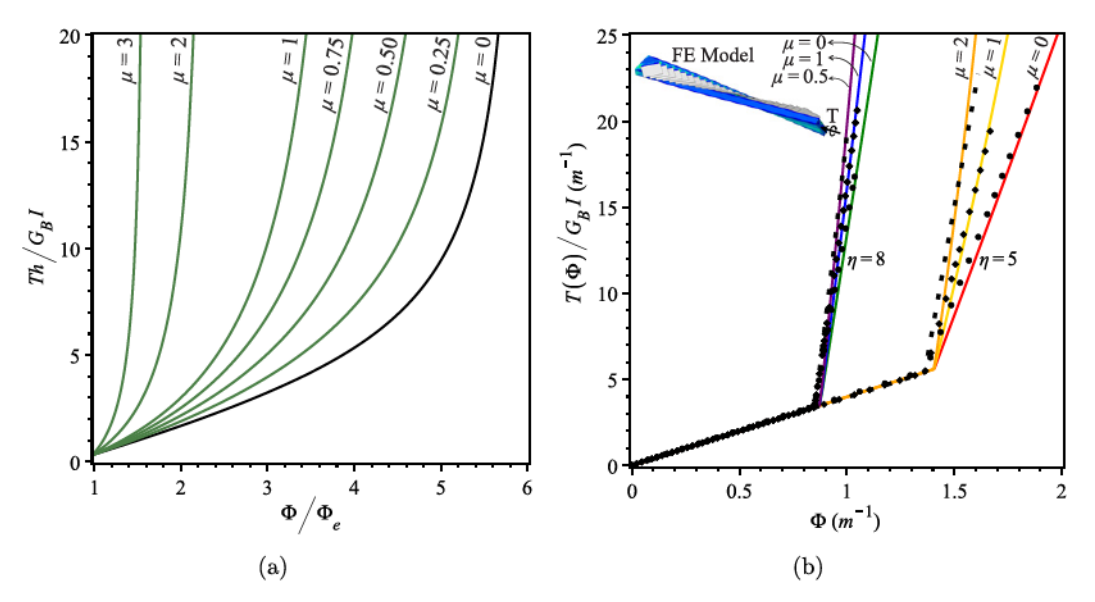


Figure 6. Torque—twist rate curve derived from (5) for different cases: (a) non-dimensionalized post-engagement torque—twist rate curves for various coefficients of friction with the given values of $\eta=3$, $\theta_0=10^\circ$, $\alpha=45^\circ$, $\beta=1.25$, $\lambda=0.45$, $\zeta=0.35$, and $L/t_s=35$, showing the perceptible effect of friction in the effective torsional stiffness of the biomimetic scale-covered structure. Here h is the substrate's thickness (h = 2t). (b) Verification of analytical model using numerical results through the plot of $T(\Phi)/G_BI$ versus twist rate (Φ) for various coefficients of friction and two different η with the given values of $\theta_0=10^\circ$, $\alpha=45^\circ$, $\beta=0.6$, $\lambda=0.32$, $\zeta=0.18$, and $L/t_s=45$. Black dotted lines represent FE results.

The proportion of lost energy is a critical quantity of interest in typical inelastic materials such as polymers and metals [65, 66]. Such losses are typically material properties, which are dependent on molecular or crystal structure. Thus, they tend to vary drastically across material classes. This lost proportion is useful in designing damping structures or determine possible temperature rise during loading. For biomimetic fish scale structures currently under study, the fundamental nature of this loss is geometric in origin. Therefore, we can tailor this loss from geometric arrangement of scales. Such tailorability can be of great interest in designing structures that can lie within acceptable range of energy dissipation.

Interestingly, in our structure, the frictional forces may not always lead to increase lost work, since friction can also decrease range of motion. In order to quantify the dual contribution of friction, we investigate the frictional work during twisting by using the RED, described in (7). According to the geometric origins of friction, the scale overlap ratio η and the oblique angle α come into the play. We set our analysis by fixing all parameters involved in RED, except μ , η , and α . This leads to contour plots shown in figure 7. In these contour plots, we have considered $\theta_0 = 10^\circ$, $\beta = 1.25$, $\lambda = 0.45$, $\zeta = 0.35$, $L/t_s = 35$, and the substrate's properties as follows $E_{\rm B} = 25$ GPa, $\nu = 0.25$, and the cross section dimension of 32 × 16 mm.

In figure 7(a), we consider $\alpha = 45^{\circ}$ to obtain an energy dissipation contour plot spanned by η and μ . This plot indicates that RED increases for higher μ ,

and also increases very slightly with η . This contour plot shows that η does not have as strong effect as coefficient of friction, on frictional energy dissipation of the system. Thus, for this oblique configuration, interscale sliding friction dominates overall dissipation. In fact, beyond a certain coefficient of friction, the increment in lost work is minimal. Thus, while designing the system, it would serve little to aim for very high frictional coefficients. However, this plot alone is an incomplete description of the problem since it may be an artifact of particular oblique configuration. Therefore, in the next figure, figure 7(b), we fix $\eta = 3$ varying α and μ . Here, we find that until some value of α , the effect of increase in friction coefficient leads to higher proportion of energy loss at intermediate μ . This finding indicates that for very rough surfaces, locking begins to severely limit the range of motion and thus overall frictional work in a cycle. This is consistent with bending analogs [42]. However, as α increases to beyond 40°, this intermediate maxima effect begins to disappear, appearing again at higher (> 60°) angles. This is a surprising result and shows how the obliqueness can be tuned to get frictional behavior as desired. This plot also shows that very low frictional coefficients (quasismooth regime) leads to low energy loss no matter what the oblique angle is. However, the geometrical effects from the angle dramatically amplify frictional effects even when frictional coefficients increase moderately. The white region in this contour plot is related to the instantaneous post-engagement frictional locking, which happens at lower α and higher μ . At this

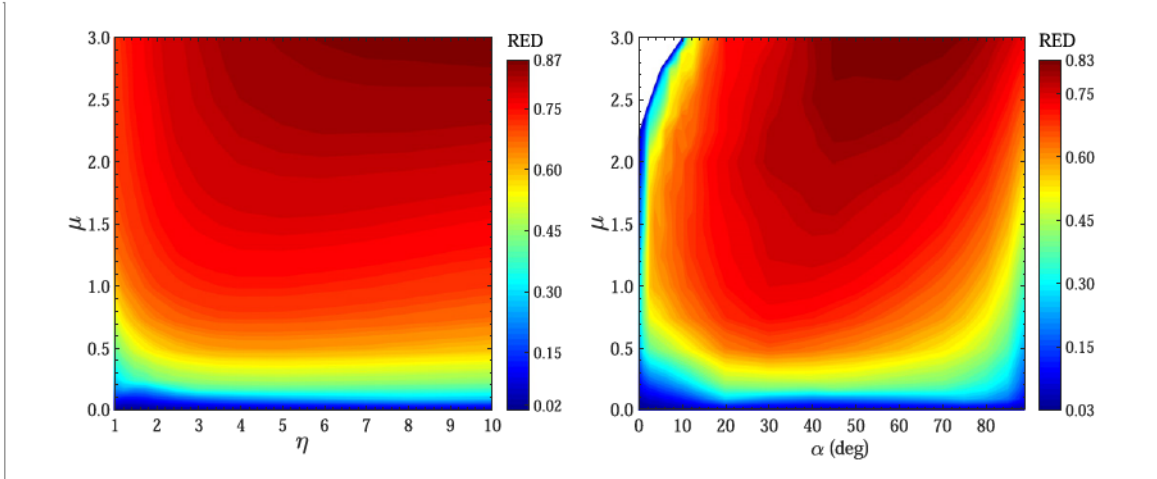


Figure 7. Non-dimensional RED factor contour plot with given values of $\theta_0 = 10^\circ$, $\beta = 1.25$, $\lambda = 0.45$, $\zeta = 0.35$, $L/t_s = 35$, $E_B = 25$ GPa, $\nu = 0.25$, and the substrate's cross section of 32 × 16 mm for two different cases: (a) spanned by μ and η by fixing $\alpha = 45^\circ$; and (b) spanned by μ and α by fixing $\eta = 3$.

condition, the system locks statically at the engagement point and the friction force does not work on the system.

5. Conclusion

We investigate for the first time, the effect of Coulomb friction on the twisting response of a biomimetic beam using a combination of analytical model and FE simulations. We established the extent and limits of universality of frictional behavior across bending and twisting regimes. The analytical model would help in obviating the need for full-scale FE simulations, which are complicated for large number of scales and for large deflection. We find that several aspects of the mechanical behavior show similarity to rough bending case investigated earlier [2]. At the same time, critical differences in response were observed, most notably the effect of the additional oblique angle. This work shows the dual contribution of frictional forces on the biomimetic scale-covered system, which includes advancing the locking envelope and at the same time increasing the torsional stiffness. Interestingly, if the coefficient of friction is large enough for a given configuration, it can lead to the instantaneous post-engagement frictional locking known as the static friction locking. This investigation demonstrates that engineering of the scale's surfaces, which produce wide range of coefficients of friction, can play an important role in tailoring the deformation response of biomimetic scale-covered systems under a variety of applications.

Our investigation shows the possibility of using surface roughness to tailor stiffness and dissipation behavior during twisting of biomimetic scale-covered substrates. Thus, a wide range and characteristic of friction behavior can arise by specially engineering surfaces of the scales. Combined with scale geometry, scale orientation, substrate combinations and distribution can potentially provide highly tailorable behavior, unprecedented for conventional substrates.

Acknowledgments

This work was supported by the United States National Science Foundation's Civil, Mechanical, and Manufacturing Innovation, CAREER Award #1943886.

Appendix A. Derivation of nonlinear kinematic relationship between the substrate local twist angle φ and the scale inclination angle θ

To find a contact criterion between 1st scale and 2nd scale, the 3D-equations of lines C_1B_1 and D_2C_2 would be established. We place the coordinates XYZ on the midpoint of 1st scale's width as shown in figure 2. Then we place coordinates xyz on the torsion axis at point O = (0, -t, 0) measured from the coordinates XYZ. Hereafter, coordinates xyz is our reference frame. Note that we do not show coordinates xyz and scale's thickness t_s in figure 2(b) to avoid visual complexity. We establish local coordinates on each scale, denoted as 'local coordinates of ith scale', and coordinates origin is located on the corner of the scale at point D_i . In these local coordinates, the unit vector of x-axis (n_{Xi}) is on the edge D_iC_i , the unit vector of y-axis (n_{Yi}) is on the edge D_iA_i , and the unit vector of z-axis (n_{Zi}) is out of plane and perpendicular to n_{Xi} and n_{Yi} , figure 2(b). On each scale, edges D_iC_i and A_iB_i are parallel and in direction of n_{Xi} , and edges C_iB_i and D_iA_i are parallel and in direction of n_{Yi} . Point M_i is located in the middle of edge C_iB_i . Using these established coordinate systems, symmetric equations of line C_1B_1 of 1st scale is as follows [67]:

$$\frac{x - x_{M_1}}{x_{n_{Y_1}}} = \frac{y - y_{M_1}}{y_{n_{Y_1}}} = \frac{z - z_{M_1}}{z_{n_{Y_1}}},$$
 (A.1)

where $n_{Y1} = (x_{n_{Y1}}, y_{n_{Y1}}, z_{n_{Y1}})$. By putting (A.1) equal to p and using geometrical parameters in figure 2, we will have parametric form of the equation of line C_1B_1 as follows, where p can vary from -b to b:

$$x(p) = p \cos \alpha - l \sin \alpha \cos \theta,$$
 (A.2)

$$y(p) = t + l\sin\theta,\tag{A.3}$$

$$z(p) = p \sin \alpha + l \cos \alpha \cos \theta.$$
 (A.4)

Point D_i is located at one end of the edge D_iC_i . Symmetric equations of line D_2C_2 of 2nd scale is as follows:

$$\frac{x - x_{D_2}}{x_{n_{X2}}} = \frac{y - y_{D_2}}{y_{n_{X2}}} = \frac{z - z_{D_2}}{z_{n_{X2}}},$$
 (A.5)

where $n_{X2} = (x_{n_{X2}}, y_{n_{X2}}, z_{n_{X2}})$. To find parametric equation of the line D_2C_2 , which is on the 2nd scale rotating with angle φ about torsion axis, first we locate the corners of 2nd scale as shown in figure 2(a), and then their locations are found after rotation, using rotation matrix. Therefore, rotated local coordinates on this scale and the unit vector in direction D_2C_2 (n_{X2}) can be established. By using these geometrical parameters and putting (A.5) equal to q, we have parametric form of the equation of line D_2C_2 as follows, where q can vary from 0 to l:

$$x(q) = (\tan \theta \tan \varphi - \sin \alpha)q$$
$$+ (t \sin \varphi - b \cos \alpha \cos \varphi), \qquad (A.6)$$

$$y(q) = (\tan \theta + \sin \alpha \tan \varphi)q$$
$$+ (t \cos \varphi + b \cos \alpha \sin \varphi), \qquad (A.7)$$

$$z(q) = \left(\frac{\cos \alpha}{\cos \varphi}\right) q + (d - b\sin \alpha). \tag{A.8}$$

To find a contact point between these two lines, (2) and (4) must be identical at x, y and z coordinate simultaneously. By putting (A.2) equal to (A.6) and also (A.3) equal to (A.7) simultaneously, we arrive at the following systems of equations:

$$\begin{bmatrix} x_{n_{Y1}} & -x_{n_{X2}} \\ y_{n_{Y1}} & -y_{n_{X2}} \end{bmatrix} \begin{bmatrix} p \\ q \end{bmatrix} = \begin{bmatrix} x_{C_2} - x_{M_1} \\ y_{C_2} - y_{M_1} \end{bmatrix}.$$
 (A.9)

Solving (A.9) will lead to equations for p and q. It yields an analytical relationship between φ and θ , by substituting the derived equation of p or q into the (A.4) or (A.8). To represent a general form for this relationship, we define dimensionless geometric parameters including $\eta = l/d$, $\beta = b/d$, and $\lambda = t/d$ as the overlap ratio, dimensionless scale width, and dimensionless substrate thickness, respectively. The governing nonlinear relationship between the substrate local twist angle φ and the scale inclination angle θ can be written as:

$$(\cos \varphi - 1) \left(\beta \sin 2\alpha \sin \theta + \eta \cos^2 \alpha \sin 2\theta + 2\lambda \cos 2\alpha \cos \theta\right) - 2\cos \alpha \cos \varphi \sin \theta + 2\sin \alpha \sin \varphi (\eta + \lambda \sin \theta) + 2\cos \alpha \sin \varphi \cos \theta (\beta - \sin \alpha) = 0. \quad (A.10)$$

By substituting derived equation of p or q into the (A.2)-(A.4) or (A.6)-(A.8), we will obtain the location of point P_{12} as the intersection between lines D_2C_2 and C_1B_1 . We can use the same procedure to establish the locations of zeroth scale's corners and its local coordinates after rotating with angle $-\varphi$ about torsion axis. We find the same nonlinear relationship between φ and θ as shown in (A.10) due to the periodicity of the system, then we can find the location of point P_{10} as the intersection between lines D_1C_1 and C_0B_0 , using the same method.

Appendix B. Derivation of parameters of scales relative motion

To describe the relative motion between zeroth scale and 1st scale, we would need the relative motion of contact point P_{10} on the edge D_1C_1 and edge C_0B_0 . Motion of point P_{10} on the edge D_1C_1 can be described as the change in the length of vector $P_{10}C_1$, which is always in direction of n_{X1} , and the change in the length of vector $P_{10}C_0$, which is always in direction of n_{Y0} . By using the superposition principle, the total differential displacement of point P_{10} can be described in vectorial format as $dR_{10} = \left(\frac{d|P_{10}C_1|}{n_{Y0}}\right)n_{X1} + \left(\frac{d|P_{10}C_0|}{n_{Y0}}\right)n_{Y0}$, figure 3. The unit vector n_{Y0} can be described in the local coordinate established on 1st scale as follows:

$$n_{Y0} = (n_{Y0}.n_{X1})n_{X1} + (n_{Y0}.n_{Y1})n_{Y1} + (n_{Y0}.n_{Z1})n_{Z1}.$$
(B.1)

By projecting n_{Y0} on the 1st scale plane, we can describe relative motion of zeroth scale with respect to 1st scale as the planar relative displacement, as follows:

$$dr = (d|P_{10}C_1| + d|P_{10}C_0|(n_{Y0}.n_{X1})) n_{X1} + (d|P_{10}C_0|(n_{Y0}.n_{Y1})) n_{Y1}.$$
 (B.2)

The length of (B.2) can be described as the relative differential displacement value:

$$\mathrm{d}r = |\mathrm{d}r| = \sqrt{\left(\mathrm{d}|P_{10}C_1| + \mathrm{d}|P_{10}C_0|(\textit{n}_{Y0}.\textit{n}_{X1})\right)^2 + \left(\mathrm{d}|P_{10}C_0|(\textit{n}_{Y0}.\textit{n}_{Y1})\right)^2}.$$
 (B.3)

To find the angle between the friction force $f_{\rm fr}$ acting in the plane of 1st scale and the unit vector n_{X1} , we can use (B.2) and (B.3) as the relative displacement vector and its value, then angle χ_{10} is derived as:

$$\chi_{10} = \arccos\left(\frac{1}{dr} \left(d|P_{10}C_1| + d|P_{10}C_0|(n_{Y0}.n_{X1}) \right) \right). \tag{B.4}$$

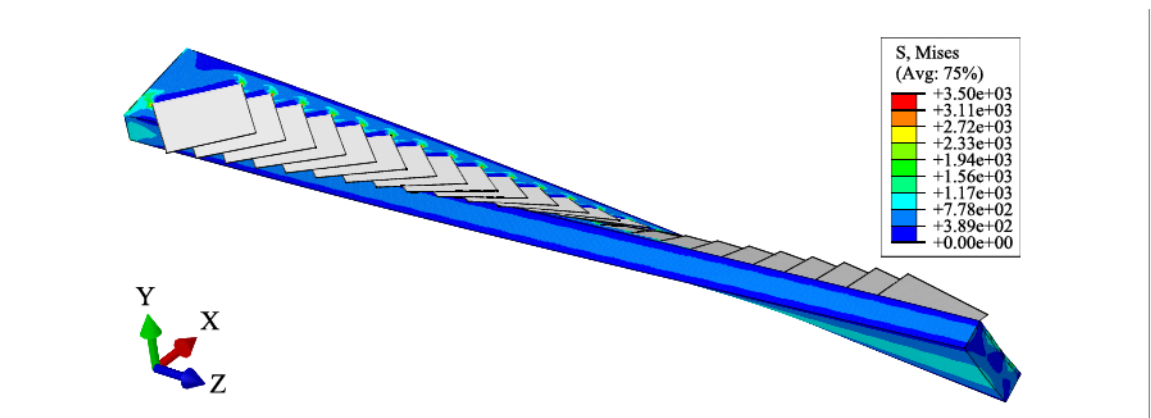


Figure C1. Contour plot of von Mises stress in a twisted scale-covered beam with deformation scale factor 1. The unit for stress is MPa in this contour plot.

If we repeat similar steps for the relative motion between 1st scale and 2nd scale, it will lead to the similar relationship for the angle between the friction force $f_{\rm fr}$ acting in the plane of 2nd scale and the unit vector n_{X2} . Finally by computing the values of these relationships, we find that $\chi_{10}=\chi_{12}$, and can be shown as χ . This finding also conforms the periodicity in the system.

Appendix C. Stress and deformation obtained by FE simulation

The FE simulations of twisting of a scale-covered beam was carried out using commercially available software ABAQUS/CAE 2017 (Dassault Systèmes). An assembly was made including two different 3D deformable solids including rectangular prismatic substrate and the scales. Then we applied rigid body constraint on the scales obviating any need for material properties for scales. In this model, a sufficient long rectangular linear elastic beam considered to satisfy periodicity. The twisting load was applied on the right end of beam cross section and the other end was fixed as shown in the figure C1. The contact mechanics was modeled using the self-contact option for the entire structure, with a defined coefficient of friction between every two neighboring scales for each simulation. The following figure shows a contour plot of von Mises stress in a twisted scale-covered beam with deformation scale factor 1. The geometrical parameters of the structure are as follows $\eta = 3$, $\theta_0 = 10^{\circ}$, $\alpha = 45^{\circ}$, $\beta = 1.25$, $\lambda = 0.45$, $\zeta = 0.35$, in the following figure.

ORCID iDs

Hossein Ebrahimi https://orcid.org/0000-0002-2672-1936

Hessein Ali D https://orcid.org/0000-0002-2420-8899

Ranajay Ghosh https://orcid.org/0000-0002-8419-9621

References

- Vernerey F J and Barthelat F 2010 Int. J. Solids Struct. 47 2268-75
- [2] Ghosh R, Ebrahimi H and Vaziri A 2014 Appl. Phys. Lett. 105 233701
- [3] Vernerey F J, Musiket K and Barthelat F 2014 Int. J. Solids Struct. 51 274–83
- [4] Ali H, Ebrahimi H and Ghosh R 2019 Int. J. Solids Struct. 166 22-31
- [5] Ali H, Ebrahimi H and Ghosh R 2019 Mech. Soft Mater. 1 10
- [6] Ebrahimi H, Ali H, Horton R A, Galvez J, Gordon A P and Ghosh R 2019 Europhys. Lett. 127 24002
- [7] Gibson L J and Ashby M F 1999 Cellular Solids: Structure and Properties (Cambridge: Cambridge University Press)
- [8] Gibson L J, Ashby M F and Harley B A 2010 Cellular Materials in Nature and Medicine (Cambridge: Cambridge University Press)
- [9] Schaedler T A, Jacobsen A J, Torrents A, Sorensen A E, Lian J, Greer J R, Valdevit L and Carter W B 2011 Science 334 962-5
- [10] Mousanezhad D, Ebrahimi H, Haghpanah B, Ghosh R, Ajdari A, Hamouda A and Vaziri A 2015 Int. J. Solids Struct. 66 218–27
- [11] Bertoldi K, Vitelli V, Christensen J and van Hecke M 2017 Nat. Rev. Mater. 2 1–11
- [12] Dell'Isola F and Steigmann D J 2020 Discrete and Continuum Models for Complex Metamaterials (Cambridge: Cambridge University Press)
- [13] Mousanezhad D, Babaee S, Ghosh R, Mahdi E, Bertoldi K and Vaziri A 2015 Phys. Rev. B 92 104304
- [14] Meyers M A, Lin A Y, Seki Y, Chen P Y, Kad B K and Bodde S 2006 JOM 58 35—41
- [15] Aizenberg J, Weaver J C, Thanawala M S, Sundar V C, Morse D E and Fratzl P 2005 Science 309 275–8
- [16] Praet T, Adriaens D, Cauter S V, Masschaele B, Beule M D and Verhegghe B 2012 Int. J. Numer. Methods Biomed. Eng. 28 1028–42
- [17] Huang J, Wang X and Wang Z L 2006 Nano Lett. 6 2325-31
- [18] Dou Z, Wang J and Chen D 2012 J. Bionic Eng. 9 457-64
- [19] Onozato H and Watabe N 1979 Cell Tissue Res. 201 409-22
- [20] Chang C, Wu P, Baker R E, Maini P K, Alibardi L and Chuong C M 2009 Int. J. Dev. Biol. 53 813
- [21] Di-Poï N and Milinkovitch M C 2016 Sci. Adv. 2 e1600708
- [22] Chen I H, Kiang J H, Correa V, Lopez M I, Chen P Y, McKittrick J and Meyers M A 2011 J. Mech. Behav. Biomed. Mater. 4 713–22
- [23] Wang B, Yang W, Sherman V R and Meyers M A 2016 Acta Biomater. 41 60–74
- [24] Yang W, Chen I H, Gludovatz B, Zimmermann E A, Ritchie R O and Meyers M A 2013 Adv. Mater. 25 31–48
- [25] Ning G, Li T, Yan J, Xu C, Wei T and Fan Z 2013 Carbon 54 241–8

- [26] Rudykh S, Ortiz C and Boyce M C 2015 Soft Matter 11 2547-54
- [27] Fratzl P and Weinkamer R 2007 Prog. Mater. Sci. 52 1263-334
- [28] Lakes R 1993 Nature 361 511
- [29] Buehler M J 2006 Proc. Natl Acad. Sci. 103 12285-90
- [30] Ortiz C and Boyce M C 2008 Science 319 1053-4
- [31] Bruet B J, Song J, Boyce M C and Ortiz C 2008 Nat. Mater. 7 748
- [32] Nelms M, Hodo W and Rajendran A 2017 J. Mech. Behav. Biomed. Mater. 69 395–403
- [33] Sire J Y, Donoghue P C and Vickaryous M K 2009 J. Anat. 214 409–40
- [34] Vickaryous M K and Sire J Y 2009 J. Anat. 214 441-64
- [35] White Z W and Vernerey F J 2018 Bioinspiration Biomimetics 13 041004
- [36] Zimmermann E A, Gludovatz B, Schaible E, Dave N K, Yang W, Meyers M A and Ritchie R O 2013 Nat. Commun. 4 2634
- [37] Ehrlich H 2015 Materials design principles of fish scales and armor Biological Materials Of Marine Origin (Berlin: Springer) pp 237–62
- [38] Browning A, Ortiz C and Boyce M C 2013 J. Mech. Behav. Biomed. Mater. 19 75–86
- [39] Funk N, Vera M, Szewciw L J, Barthelat F, Stoykovich M P and Vernerey F J 2015 ACS Appl. Mater. Interfaces 7 5972–83
- [40] Martini R and Barthelat F 2016 Bioinspiration Biomimetics 11 066001
- [41] Vernerey F J and Barthelat F 2014 J. Mech. Phys. Solids 68 66–76
- [42] Ghosh R, Ebrahimi H and Vaziri A 2016 Europhys. Lett. 113 34003
- [43] Ghosh R, Ebrahimi H and Vaziri A 2017 J. Mech. Behav. Biomed. Mater. 72 1–5
- [44] Ali H, Ebrahimi H and Ghosh R 2019 Sci. Rep. 9 14628
- [45] Ali H, Ebrahimi H, Stephen J, Warren P and Ghosh R 2020 Tailorable stiffness lightweight soft robotic materials with architectured exoskeleton AIAA Scitech 2020 Forum p 1551
- [46] Hebrank M R and Hebrank J H 1986 Biol. Bull. 171 236
- [47] Westneat M W and Wainwright S A 2001 Fish Physiol. 19 271–311
- [48] Rousseaux C 2013 Energetic Science and Piranha-Proof Armor https://science.osti.gov/Science-Features/News-Archive/Featured-Articles/2013/12-12-13(accessed May 19, 2020)

- [49] Miller G S 1988 The motion dynamics of snakes and worms Proc. of the 15th Annual Conf. on Computer Graphics and Interactive Techniques pp 169–73
- [50] Khan R, Watanabe M, Shafie A et al 2010 Am. J. Appl. Sci. 7 669
- [51] Marvi H and Hu D L 2012 J. R. Soc. Interface 9 3067-80
- [52] Praet T, Adriaens D, Cauter S V, Masschaele B, Beule M D and Verhegghe B 2012 Int. J. Numer. Methods Biomed. Eng. 28 1028–42
- [53] Porter M M, Novitskaya E, Castro-Ceseña A B, Meyers M A and McKittrick J 2013 Acta Biomater. 9 6763–70
- [54] Porter M M, Adriaens D, Hatton R L, Meyers M A and McKittrick J 2015 Science 349 aaa6683
- [55] Steltz E, Mozeika A, Rembisz J, Corson N and Jaeger H 2010 Jamming as an enabling technology for soft robotics Electroactive Polymer Actuators and Devices (EAPAD) 2010 vol 7642 (International Society for Optics and Photonics) p 764225
- [56] Sadati S H, Noh Y, Naghibi S E, Kaspar A and Nanayakkara T 2015 Stiffness control of soft robotic manipulator for minimally invasive surgery (MIS) using scale jamming Int. Conf. on Intelligent Robotics and Applications (Springer) pp 141–51
- [57] Wei Y, Chen Y, Ren T, Chen Q, Yan C, Yang Y and Li Y 2016 Soft Robot. 3 134–43
- [58] Schneider F, Fellner T, Wilde J and Wallrabe U 2008 J. Micromech. Microeng. 18 065008
- [59] Pan Y, Zhu F, Fan J, Tao J, Lin X, Wang F and Shi L 2018 Polymers 10 195
- [60] Cliff C 2007 Arapaima (arapaima Gigas) Online Image, Flickr https://flickr.Com/photos/nostri-Imago/ 2891841621(accessed June 2, 2020)
- [61] Barrett R T 1990 Fastener Design Manual vol 1228 (NASA, Scientific and Technical Information Division)
- [62] Gnecco E and Meyer E 2015 Elements of Friction Theory and Nanotribology (Cambridge: Cambridge University Press)
- [63] Ugural A C and Fenster S K 2011 Advanced Mechanics of Materials and Applied Elasticity (Boston, MA: Pearson Education)
- [64] Waghmare P R, Gunda N S K and Mitra S K 2014 Sci. Rep. 4 7454
- [65] Boschung E, Heuberger M and Dietler G 1994 Appl. Phys. Lett. 64 3566-8
- [66] Jiang M, Ling Z, Meng J and Dai L 2008 Phil. Mag. 88 407–26
- [67] George T B and Finney R 1988 Calculus and Analytic Geometry (Reading, MA: Addison-Wesley)